Modern Mechanical Engineering, 2026, 16(3), 67-82
https://www.scirp.org/journal/mme
ISSN Online: 2164-0181
ISSN Print: 2164-0165

Optimization of P & O MPPT Tracking under Thermal Constraints: Sensitivity Analysis of the Perturbation Step ΔD for a PV-Boost System

Sada Traore[1,2*], Moustapha Thiame[2], Ansoumane Diedhiou[2], Modou Tine[2]

[1]Laboratory of Semiconductor and Solar Energy, Cheikh Anta Diop University, Dakar, Senegal
[2]Laboratory of Chemical and Physics of Materials, Assane Seck University, Ziguinchor, Senegal
Email: *sadatraore59@yahoo.fr

How to cite this paper: Traore, S., Thiame, M., Diedhiou, A. and Tine, M. (2026) Optimization of P & O MPPT Tracking under Thermal Constraints: Sensitivity Analysis of the Perturbation Step ΔD for a PV-Boost System. *Modern Mechanical Engineering*, **16**, 67-82.
https://doi.org/10.4236/mme.2026.163004

Received: May 13, 2026
Accepted: July 28, 2026
Published: July 31, 2026

Abstract

This paper presents a detailed optimization of the Perturb and Observe (P & O) Maximum Power Point Tracking (MPPT) algorithm applied to a 250 W photovoltaic module connected to a DC-DC Boost converter. The main contribution lies in a systematic sensitivity analysis of the perturbation step size (ΔD) under severe thermal constraints ranging from 25˚C to 70˚C. The PV module was modeled using the single-diode equivalent circuit, while the Boost converter was designed and simulated in Continuous Conduction Mode (CCM) using the averaged state-space approach in MATLAB/Simulink. Simulation results demonstrate that the choice of ΔD is critical: a too-small step ($\Delta D < 0.002$) leads to excessively slow convergence (>2.5 s), whereas a too-large step ($\Delta D > 0.015$) causes significant steady-state oscillations and reduces tracking efficiency below 92%. The optimal perturbation step $\Delta D = 0.005$ achieves an excellent compromise, providing an average tracking efficiency of 96.80% and a convergence time of 1.2 s. Compared to open-loop control with fixed duty cycle, the optimized P & O MPPT delivers an average power gain of +25.6%, reaching up to +39.3% at 25˚C.

Keywords

P & O MPPT, Sensitivity Analysis, Perturbation Step ΔD, Boost Converter, Thermal Constraints, MATLAB/Simulink

1. Introduction

The growing demand for clean energy has fostered the development of photovoltaic (PV) systems, recognized for their renewable nature and low environmental impact [1] [2]. However, the current-voltage (I-V) characteristic of a PV module is inherently nonlinear and presents a unique maximum power point (MPP), whose position fluctuates with irradiance and temperature [3] [4]. To address this challenge, Maximum Power Point Tracking (MPPT) algorithms are essential for continuously extracting optimal power from the generator [5].

Among these methods, the Perturb and Observe (P & O) algorithm remains the most widely used due to its simplicity of implementation and its reliability in steady-state operation [6] [7]. Combined with a Boost converter, this algorithm dynamically adjusts the duty cycle D to maintain the operating point at the MPP [8] [9]. Although these advantages are well recognized, most studies on this algorithm share a notable limitation. Research on fixed-step P & O methods has largely concentrated on irradiance variations [10], while adaptive (variable step-size) techniques adjust ΔD in real time without quantifying the impact of temperature on the optimal fixed step size. To date, very few works offer a comprehensive quantitative analysis of how the optimal perturbation step ΔD evolves across a wide temperature range (25 - 70˚C), despite temperature being a critical driver of MPP drift in real-world operating conditions.

The present work aims to address this gap by proposing a temperature-sensitive design rule for selecting ΔD under a constant irradiance of 1000 W/m^2 (STC conditions).

The contributions of this article are structured around four main axes:

1) Accurate modeling of a 250 W PV module using the single-diode model;

2) Design of a Boost converter operating in Continuous Conduction Mode (CCM) under MATLAB/Simulink;

3) Quantitative evaluation of P & O performance under thermal constraints;

4) Sensitivity analysis of the perturbation step ΔD;

5) Comparative analysis with open-loop control.

2. Photovoltaic Module Modeling

2.1. Single-Diode Equivalent Circuit

In this modeling approach, the single-diode equivalent photovoltaic model is adopted. This model offers the best trade-off between accuracy and computational complexity [11] [12]. The generalized I-V relationship for a module with Ns series-connected cells is:

$$I = I_{ph} - I_0\left(\exp\left(\frac{\left(V + R_s I\right)}{n \cdot V_t \cdot N_s}\right) - 1\right) - \frac{V + R_s I}{R_{sh}} \tag{1}$$

Where I_{ph} is the photogenerated current [A], I_0 is the diode saturation current [A], n is the ideality factor, $V_t = \frac{kT}{q}$ the thermal voltage [V] with k the Boltzmann constant, q the electron charge and T the absolute temperature [K], and R_s, R_{sh} are the series and shunt resistances [Ω].

2.2. Effect of Irradiance and Temperature

The photogenerated current I_{ph} varies linearly with solar irradiance G [W/m^2] and depends on temperature T according to [13] [14]:

$$I_{ph} = \left(I_{sc_{ref}} + K_{Isc}\left(T - T_{ref}\right)\right) \cdot \frac{G}{G_{ref}} \tag{2}$$

The diode saturation current (I_0) is strongly temperature-dependent:

$$I_0 = I_{0,ref}\left(\frac{T}{T_{ref}}\right)^3 \cdot \exp\left[\frac{qE_g}{nk}\left(\frac{1}{T_{ref}} - \frac{1}{T}\right)\right] \tag{3}$$

where E_g ≈ 1.121 eV is the silicon bandgap energy. The open-circuit voltage Voc decreases with temperature at the rate $K_V \approx -0.34$ %/˚C, while the short-circuit current I_{sc} increases slightly at the rate $K_I \approx +0.065$ %/˚C.

2.3. Module Parameters and Characteristic Curves (STC)

Table 1 presents the electrical parameters of the 250 W PV module at Standard Test Conditions (STC: G = 1000 W/m^2, T = 25˚C, AM = 1.5).

The internal single-diode parameters used in the simulation are: photogenerated current I_{ph} = 8.9397 A, diode saturation current I_0 = 4855 × 10^{-10} A, ideality factor n = 1, series resistance R_s = 0.31 Ω, and shunt resistance R_{sh} = 188.26 Ω. These values were extracted from the module datasheet (Voc, Isc, Vmp, Imp, KV, KI). The simulated STC operating points (Voc, Isc, Vmp, and Imp) coincide with the datasheet values, resulting in negligible errors and confirming our simulated parameters.

Table 1. Electrical parameters of the 250 W PV module (STC).

Parameter	Symbol	Value
Nominal power	Pmp	250 W
MPP voltage	Vmp	30.0 V
MPP current	Imp	8.33 A
Open-circuit voltage	Voc	37.0 V
Short-circuit current	Isc	8.90 A
Voltage temp. coeff.	K_V	−0.34%/˚C
Current temp. coeff.	K_I	+0.065%/˚C
Series cells	Ns	60

The corresponding I-V and P-V curves are presented in Figures 1-2.

Figure 1 and Figure 2 illustrate the simulated curves of the 250 W PV module. The I-V nonlinearity and the uniqueness of the MPP at each irradiance level are clearly visible. The short-circuit current I_{sc} evolves proportionally to G, while Voc varies logarithmically. With temperature, Voc decreases significantly (−0.34%/˚C) and I_{sc} increases slightly (+0.065%/˚C), resulting in a net reduction of maximum power of approximately 0.40%/˚C.

The validation results indicate perfect agreement between the simulated and manufacturer-reported STC operating points. This outcome is expected because the single-diode parameters were extracted directly from the datasheet through an iterative fitting procedure. Therefore, the obtained model accurately reproduces the reference electrical characteristics before being used for MPPT performance evaluation.

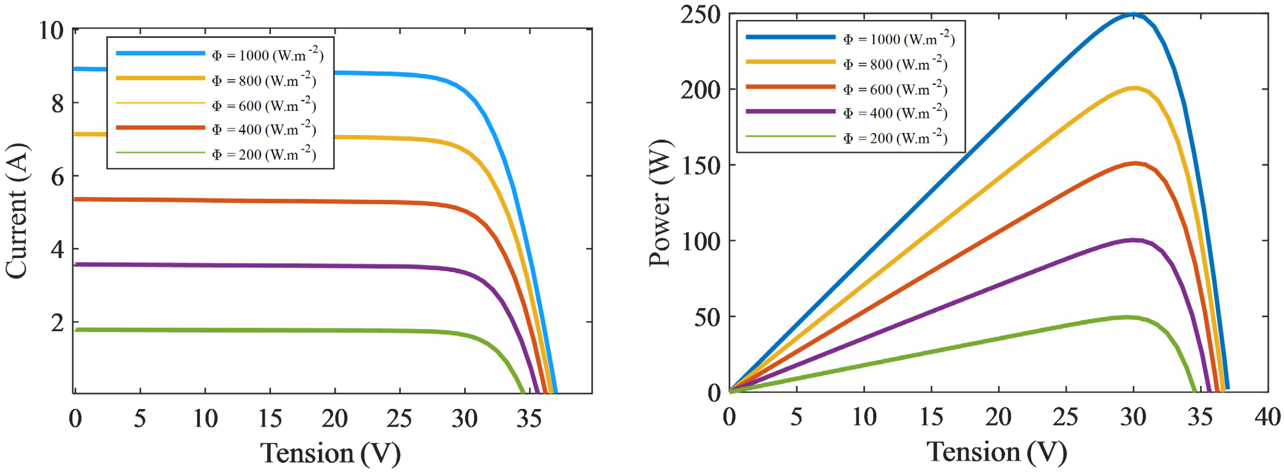

Figure 1. I-V and P-V curves at temperature T = 25˚C.

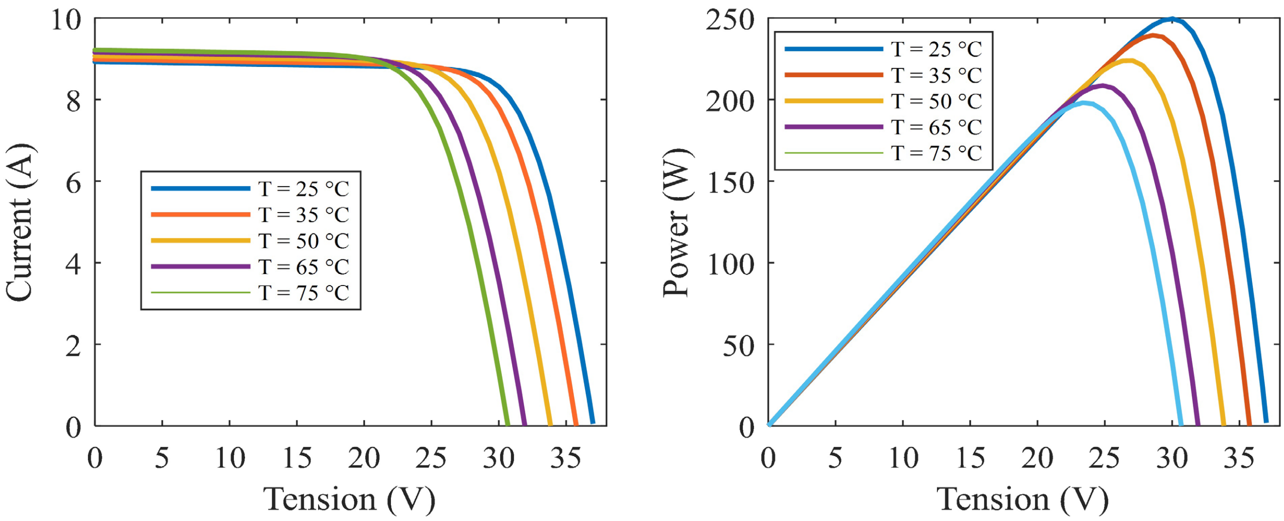

Figure 2. I-V and P-V curves at irradiance G = 1000 W/m^2.

3. Boost Converter

The DC-DC Boost converter, also known as a step-up converter, is a central element of the PV system studied in this work. It provides impedance matching between the photovoltaic generator and the load by boosting the input voltage V_{pv} to an output voltage V_{out} higher than the input, according to the conversion relationship $M(D) = 1/(1-D)$.

The schematic diagram of the Boost converter is shown in Figure 3. It consists of four main components: an inductor (L), a controlled switch (MOSFET), a diode (D), and an output capacitor (C).

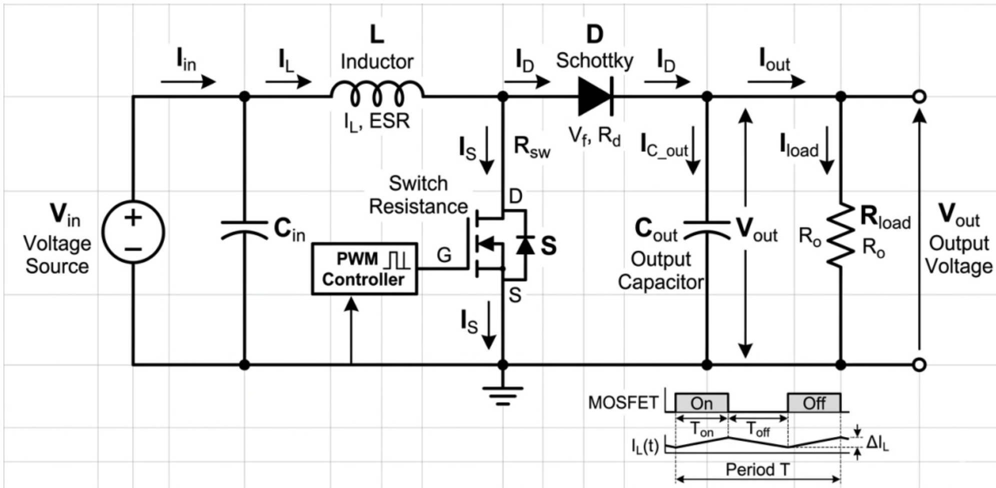

Figure 3. Electrical model of the boost converter.

The Boost converter increases the input voltage supplied by the PV generator to a higher output voltage, through the cyclic switching of a controlled switch (MOSFET) at the chopping frequency. Continuous Conduction Mode (CCM) operation is maintained throughout the operating range, ensuring that the inductor current remains strictly positive at all times.

Each switching period T_s is divided into two distinct intervals, governed by the inductor law $U_L = LdI_L/\mathrm{d}t$:

1) ON Phase $(0 \le t < D \cdot T_s)$: The MOSFET is saturated and the diode is blocked. The voltage V_{pv} is applied directly across the inductor terminals, whose current rises linearly according to $dI_L(t)/\mathrm{d}t = V_{pv}/L$. Energy is thus stored in the inductor's magnetic field, while capacitor C alone supplies the load R_L.

2) OFF Phase $(D \cdot T_s \le t < T_s)$: The MOSFET is off and the diode becomes conductive. The inductor, whose back-EMF adds to V_{PV}, transfers its energy to the load through the diode. The current I_L decreases linearly according to $dI_L/\mathrm{d}t = (V_{pv} - (V_{out})/L < 0$, while recharging capacitor C.

3.1. Averaged State-Space Equations

The dynamic modeling of the Boost converter is based on the averaged state-space method, introduced by Middlebrook and Ćuk [15] [16]. This approach consists in deriving the differential equations of the circuit for each of the two switching phases and then weighting them by the duty cycle D. This method provides a linearized model that is valid in Continuous Conduction Mode (CCM) and can be used directly for analysis and sizing [17] [18].

Applying the averaged state-space method, the equations governing the dynamic behavior of the Boost converter are:

$$\frac{di_L}{\mathrm{d}t} = \frac{V_{pv} - (1-D)\cdot V_{out}}{L} \tag{4}$$

$$\frac{dV_{out}}{\mathrm{d}t} = \frac{R(1-D)I_L - V_{out}}{RC} \tag{5}$$

In steady state, the derivatives vanish and we obtain the characteristic conversion ratio of the Boost converter:

$$M(D) = \frac{V_{out}}{V_{pv}} = \frac{1}{(1-D)} \tag{6}$$

3.2. Component Sizing

The minimum sizing of inductance L and capacitance C is performed to meet the specified ripple criteria: inductor current ripple $\mathrm{I}_L \le 5\%$ of the average inductor current I_L and output voltage ripple $\Delta V_{out} \le 1\%$ of V_{pv}.

$$L_{\min} = \frac{D\cdot(1-D)^2\cdot R_L}{2\cdot f_s} \tag{7}$$

$$C_{\min} = \frac{V_{out}\cdot D}{R_L\cdot f_s\cdot \Delta V_{out}} \tag{8}$$

The design parameters selected for the boost converter are summarized in Table 2. The values adopted in the simulation (L = 2 mH and C = 470 μF) well exceed these minimum constraints and guarantee robust CCM operation over the entire studied temperature range (25 - 70˚C).

Table 2. Boost converter design parameters.

Parameter	Symbol	Optimal value
Switching frequency	fs	20 kHz
Input voltage range	V_{PV}	15 - 35 V
Nominal output voltage	V_{out}	48 V
Inductance	L	2 mH
Output capacitance	C	470 μF
Load resistance	RL	9.2 Ω
Inductor current ripple	ΔIL	<5%
Output voltage ripple	ΔVout	<1%

4. P & O MPPT Algorithm

The P & O algorithm is based on the following observation: on the P-V curve of a PV module, the derivative $\frac{dP}{dV}$ is positive to the left of the MPP and negative to the right. At the MPP, $\frac{dP}{dV} = 0$.

By periodically perturbing the operating voltage and observing the resulting power variation (ΔP), the controller determines the direction of the next perturbation.

The decision table of the algorithm is presented in Table 3, and the corresponding flowchart in Figure 4. The duty cycle update at each sampling instant k is:

$$D(k) = D(k-1) \pm \Delta D \tag{9}$$

The perturbation step ΔD = 0.005 was identified from a sensitivity analysis performed under nominal STC conditions (T = 25˚C, G = 1000 W/m^2) as the best compromise between convergence speed and steady-state oscillations.

Table 3. Decision logic of the P & O algorithm.

Sign of ΔV	Sign of ΔP	Action on D
>0	>0	Increase D (+ΔD)
>0	<0	Decrease D (−ΔD)
<0	>0	Decrease D (−ΔD)
<0	<0	Increase D (+ΔD)

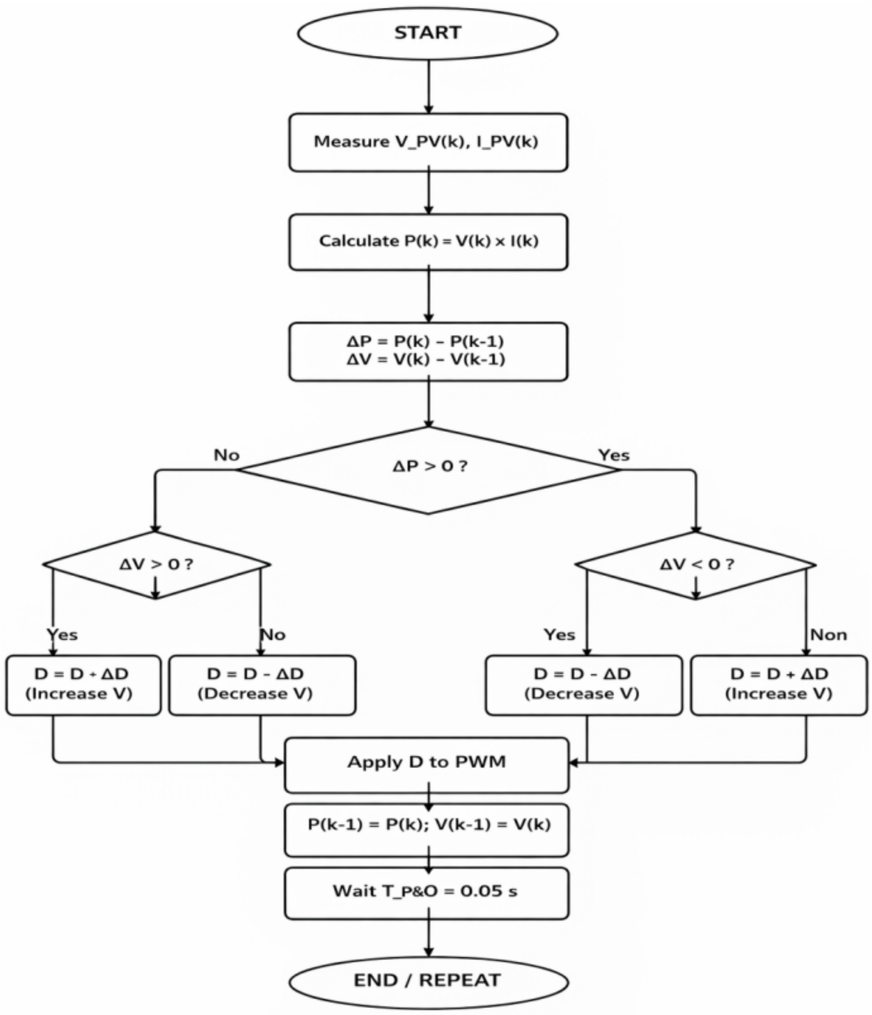

Figure 4. Flowchart of the P & O algorithm.

Figure 5 presents the complete Simulink model of the PV-Boost-MPPT system.

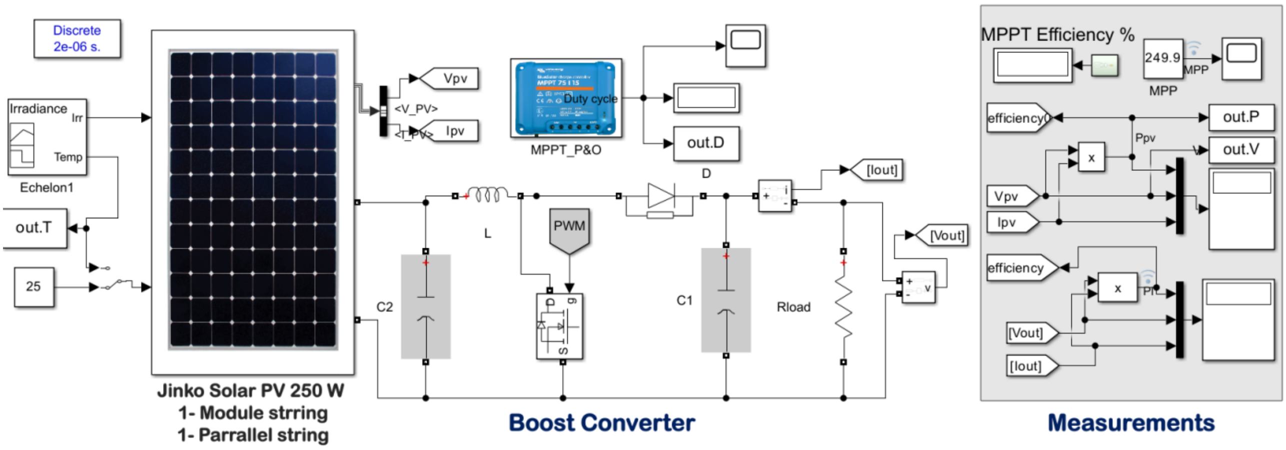

Figure 5. Simulink model for the proposed controller.

This Simulink diagram represents a photovoltaic system consisting of a Jinko 250 W solar panel connected to a Boost converter. A Perturb & Observe (P & O) MPPT algorithm is used to extract the maximum power from the panel by adjusting the duty cycle (D) of the converter.

The model includes the inputs (irradiance and temperature), the boost circuit with PWM, and a measurements block displaying power, voltage, current, and MPPT efficiency.

5. Simulation Results and Discussion

5.1. Tracking Efficiency and Sensitivity Analysis of the Duty Cycle Step ΔD

The complete PV-Boost-MPPT system was implemented in MATLAB/Simulink using the averaged state-space model of the Boost converter operating in CCM. The initial duty cycle was set to $D_0 = 0.50$. The load resistance was fixed at RL = 9.2 Ω, corresponding to a nominal output voltage of 48 V. The PWM switching frequency was fs = 20 kHz, while the MPPT sampling period was TPO = 0.05 s. Each simulation was carried out over a duration of 4 s.

5.1.1. Tracking Efficiency

Tracking efficiency (η_{MPPT}) is the main performance criterion. It represents the ratio between the energy actually extracted by the chopper (or inverter) and the maximum theoretical energy available over the simulation duration [19]:

$$\eta_{MPPT} = \frac{\int_0^{Tsim} P_{MPPT}(t)\,\mathrm{d}t}{\int_0^{Tsim} P_{MPP}(t)\,\mathrm{d}t} \times 100\% \tag{10}$$

Where T_{sim} represents the total simulation time. The reference power $P_{MPP}(t)$ was generated from the PV model by directly computing the theoretical maximum power point corresponding to the instantaneous irradiance and temperature conditions. At each simulation instant, $P_{MPP}(t)$ represents the global maximum of the P-V characteristic, whereas $P_{MPPT}(t)$ corresponds to the power extracted by the simulation.

5.1.2. Convergence Dynamics and Thermal Behavior

Over a 4 s simulation window, the system reaches steady state after approximately 24 iterations (1.2 s × 1/0.05 s) where 0.05 s corresponds to the sampling period T_{PO}.

The importance of MPPT is amplified by thermal variations. When the temperature increases from 25˚C to 70˚C, the voltage V_{MPP} decreases, shifting the optimal operating point according to:

$$V_{mpp}(T) = V_{mpp,STC} + K_V \cdot (T - T_{STC}) \cdot V_{mpp,STC} \quad (11)$$

Without MPPT (fixed D = 0.5), the system operates at a fixed point that significantly deviates from the actual MPP, producing only 179.4 W at 25˚C (183.65 W on average over the 25˚C - 70˚C range).

With active P & O MPPT, the controller dynamically adjusts the duty cycle, reaching a steady-state power of 249.9 W at 25˚C corresponding to an average tracking efficiency of 96.80%.

5.1.3. Sensitivity Analysis of Step ΔD

The choice of the perturbation step ΔD is the most critical tuning parameter of the P & O algorithm. A systematic sensitivity analysis (**Figure 6**) was carried out by varying ΔD from 0.001 to 0.030 under fixed STC conditions (G = 1000 W/m^2, T = 25˚C).

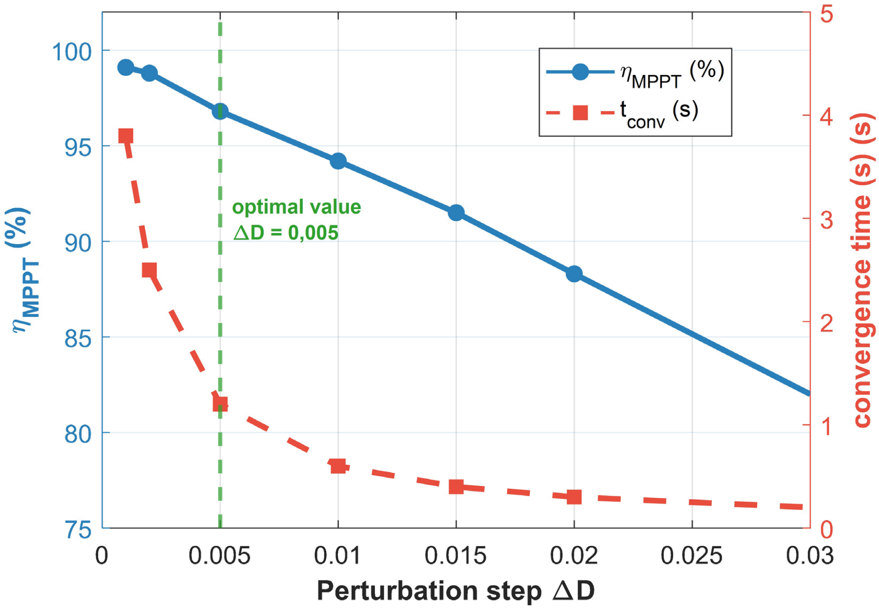

Figure 6. Impact of the perturbation step ΔD on the tracking efficiency η_{MPPT} (left axis, blue) and the convergence time t_{conv} (right axis, red). The dashed green line indicates the optimal value ΔD = 0.005 at (T = 25˚C, G = 1000 W/m^2).

The convergence time t_{conv} is defined as the first instant at which the extracted power enters and remains within ±2% of the theoretical maximum power P_{MPPP}. Similarly, the retracking time t_{retrack} is defined as the time required to return and remain within the same tolerance band after a temperature step change.

For each value, the tracking efficiency η_{MPPT} and the convergence time t_{con} were recorded at steady state (Table 4).

Table 4. Impact of step ΔD on system performance.

Step ΔD	Convergence time (t_{conv})	Stability (Steady state)	Overall efficiency
Small (<0.002)	Slow (>2.5 s)	Very stable (no oscillations)	Low (due to slowness)
Optimal (0.005)	Balanced (1.2 s)	Controlled oscillations	Maximum (96.8%)
Large (>0.015)	Fast (<0.5 s)	Strong oscillations (instability)	Degraded (<92 %)

1) Speed vs. Accuracy: When the perturbation step is too small (ΔD < 0.002), oscillations are minimized, but convergence is considerably slowed, with a response time exceeding 2.5 s.

2) Stability vs. Efficiency: Conversely, a too-large step (ΔD > 0.015) speeds up convergence but reduces efficiency below 92% due to excessive residual oscillations around the MPP.

3) Optimal Value: The optimal perturbation step ΔD = 0.005 provides the best compromise, yielding a tracking efficiency of 96.8% and a convergence time of 1.2 s under fixed STC conditions (G = 1000 W/m^2, T = 25˚C). This finding aligns with the recommendations of Femia *et al.* [20], who advise setting the step size to approximately 1/200 of the duty cycle's dynamic range to minimize steady-state oscillations while ensuring sufficient responsiveness to environmental changes.

5.2. Dynamic Performance under Temperature Step Changes

To assess the robustness of the optimal perturbation step (ΔD = 0.005), a stepwise temperature profile consisting of four levels (25˚C, 40˚C, 55˚C, and 70˚C) was applied during a 4 s simulation. Figure 7 illustrates the dynamic response of the PV power, duty cycle, and PV voltage.

1) Retracking Performance: The P & O algorithm effectively retracks the new maximum power point following each temperature change, with a re-stabilization time of 0.04 to 0.08 s per step.

2) Duty Cycle Adaptation: The controller dynamically adapts the duty cycle from D = 0.375 at 25˚C to approximately D = 0.49 at 70˚C to compensate for the reduction in MPP voltage (V_{mpp}).

In open-loop control with fixed D = 0.50, the extracted power increases slightly with temperature, from 179.4 W at 25˚C to 186.2 W at 70˚C. This phenomenon is explained by the slight increase in short-circuit current I_{sc} with T (KI = +0.065%/˚C) which shifts the intersection of the I-V curve with the fixed load line toward slightly higher voltage and current values. However, this power remains far below the theoretical MPP, which decreases from 250 W to 203.7 W over the same temperature range, fully justifying the use of P & O MPPT.

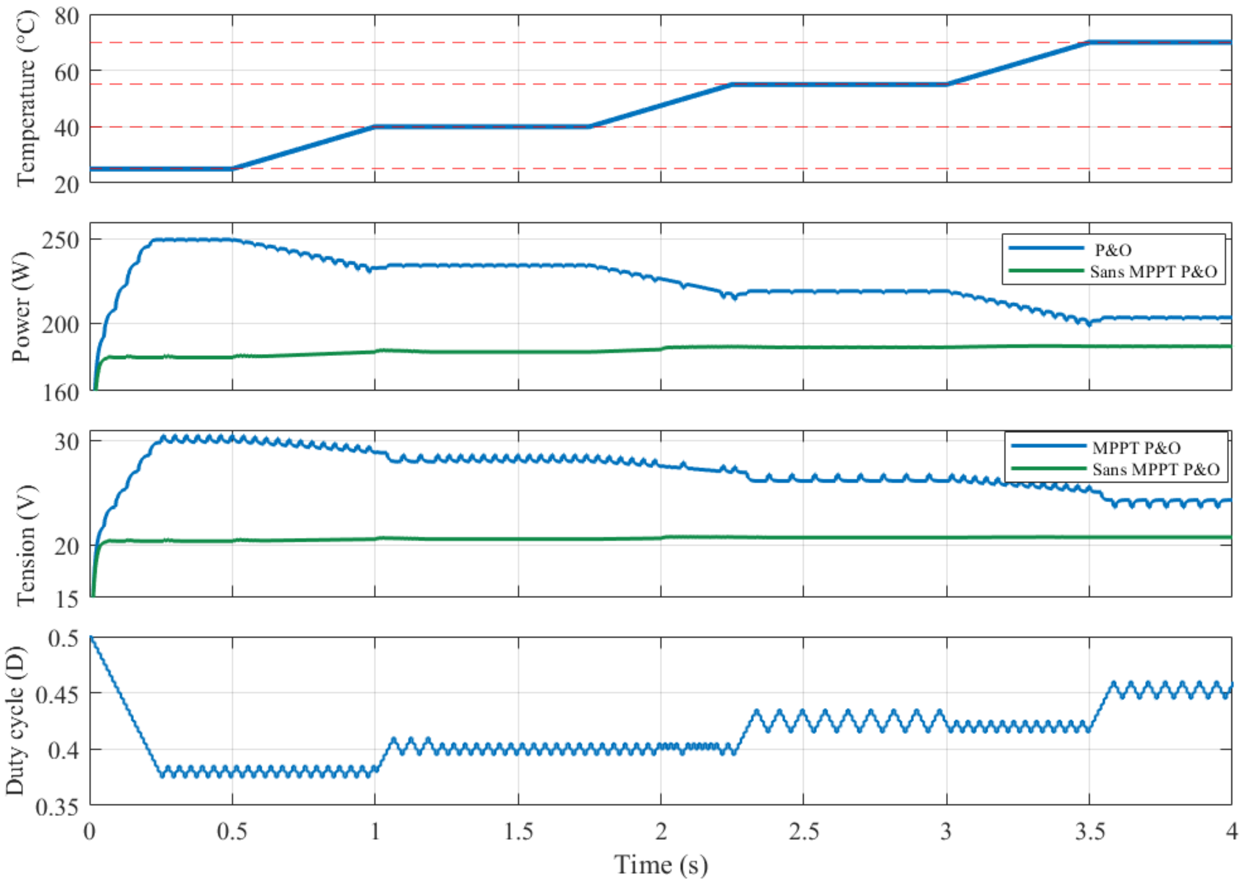

Figure 7. Dynamic response of the PV-Converter-MPPT P & O system under successive temperature steps (25˚C → 40˚C → 55˚C and 70˚C).

5.3. Comparative Performance Analysis: Optimized P & O MPPT versus Open-Loop Control

Table 5 provides a detailed quantitative comparison of the system performance under the two control configurations. Four independent simulations were performed at constant temperatures of 25˚C, 40˚C, 55˚C, and 70˚C, under constant irradiance of 1000 W/m² (STC conditions).

Table 5. Performance comparison between optimized P & O MPPT and open-loop control under thermal constraints.

T (˚C)	Theoretical MPP		without MPPT (Fixed D = 0.50)		With MPPT P & O		Duty Cycle D	Power Gain (%)
	$Vmpp(V)$	$Pmpp(w)$	$Vpv(V)$	$Ppv(w)$	$Vpv(V)$	$Ppv(w)$		
25˚C	30	249.9	20.34	179.4	30	249.9	0.375	+39.3
40˚C	28.47	234.54	20.8	182	28.14	234.9	0.41	+29.1
55˚C	26.94	219.15	21.1	187	26.3	219.4	0.45	+17.3
70˚C	25.4	203.52	20.74	186.2	24.48	203.7	0.49	+9.4
Average	—	**226.78**	—	**183.65**		**227**	**0.416**	**+25.60**

These results show that the gain provided by P & O MPPT is greater at lower temperatures.

1) Power Gain: The MPPT system delivers an average gain of +25.6% compared to a fixed duty cycle (D = 0.50).

2) Temperature Impact: At 25˚C, the gain reaches its maximum of +39.3%, underscoring the critical importance of active tracking even when available power is at its maximum.

3) Overall Efficiency: The average tracking efficiency remains at 96.80% across the entire temperature range, confirming the validity of the Boost converter component sizing (L = 2 mH, C = 470 μF) in Continuous Conduction Mode (CCM).

Figure 8 shows a histogram comparing the power gains and the overall system efficiency under different operating conditions.

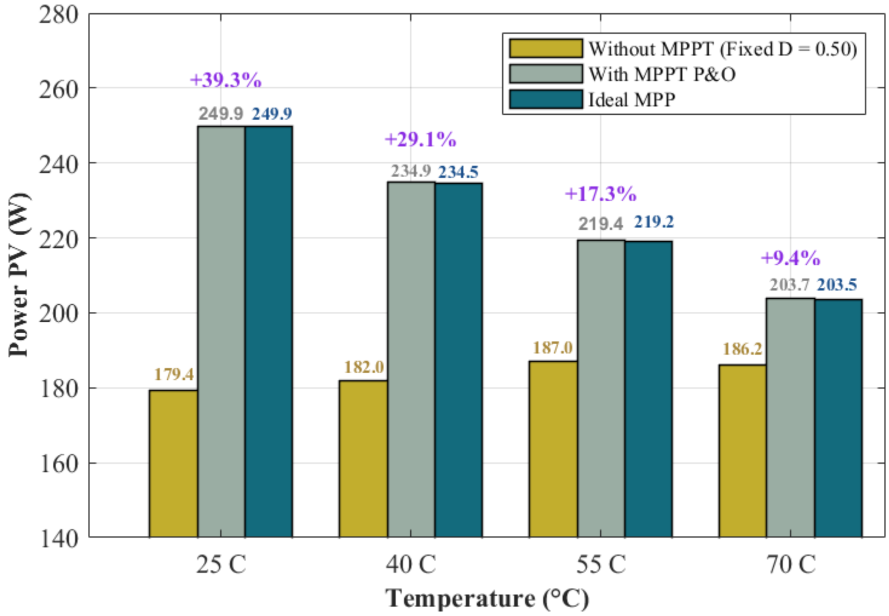

Figure 8. Comparative histogram of PV power extracted using open-loop control (fixed D = 0.50), Optimized P & O MPPT, and the theoretical maximum power point (ideal MPP) at different temperatures (G = 1000 W/m^2).

The results confirm that the P & O algorithm delivers near-optimal power extraction in steady state (average η_{MPPT} = 96.80%, ranging from 97.09% at 25˚C to 96.46% at 70˚C), which is consistent with the performances reported in the literature for similar boost converter configurations [21] [22]. The average gain of +25.6% (reaching +39.3% at 25˚C) compared to a fixed duty cycle underscores the critical importance of active tracking to maximize the energy efficiency of the photovoltaic generator [23].

The main limitation of fixed-step P & O observed in this study is the persistence of a low-amplitude oscillation around the maximum power point (P_{MPP}) in steady state. Adaptive step variants, proportional to |ΔP/ΔV|, would drastically reduce these oscillations without sacrificing convergence speed [24] [25]. Although P &

O is effective under thermal variations, its main limitation arises during rapid irradiance changes (G > 500 W/m^2), where the power variation due to the perturbation may be dominated by the environmental variation, leading to mistracking [26]. To overcome these shortcomings, artificial intelligence-based approaches, such as artificial neural networks (ANN) or fuzzy logic, offer superior dynamic performance and tracking accuracy by eliminating residual oscillations [27] [28].

6. Comparison of MPPT Techniques

Table 6 presents a comparative summary of the main MPPT techniques. Methods based on fuzzy logic [29] [30] and artificial neural networks [20] offer superior performance under partial shading and rapid variations, but at the cost of higher implementation complexity and computational burden. The PSO algorithm [31] is particularly well-suited for multi-peak configurations. Incremental conductance [32] represents a direct alternative to P & O, with better performance in transient conditions.

Table 6. Comparison of the main MPPT techniques [20] [29]-[32].

Method	Complexity	MPPT Efficiency	Convergence Speed	Steady-State Oscillation	Partial Shading	Implementation Cost
Fixed D (no MPPT)	Very low	<85%	—	None	Poor	Very low
P & O (fixed step)	Low	97 - 99%	Moderate	Lows	Poor	Low
Conductance incr. (CI)	Moderate	98 - 99.5%	Fast	Very low	Poor	Low
Fuzzy logic (FL)	High	99 - 99.8%	Very fast	Negligible	Moderate	Medium
Neural network	Very high	>99.5%	Very fast	Negligible	Good	Very high
PSO/Metaheuristics	Very high	>99%	Moderate	Lows	Excellent	High

7. Conclusions

This paper has presented a comprehensive modeling, simulation, and performance analysis of a 250 W photovoltaic system equipped with a DC-DC Boost converter and a Perturb and Observe (P & O) MPPT controller. The study focused on the optimization of the perturbation step size ΔD under wide thermal constraints ranging from 25˚C to 70˚C at constant irradiance of 1000 W/m^2.

The main findings of this work are as follows:

1) The single-diode model accurately reproduces the I-V and P-V characteristics of the PV module across the studied temperature range.

2) The Boost converter, operating in Continuous Conduction Mode (CCM) at 20 kHz with L = 2 mH and C = 470 μF, maintains output voltage ripple below 1%.

3) The systematic sensitivity analysis performed under STC conditions (25˚C, 1000 W/m^2) demonstrated that $\Delta D = 0.005$ provides the best trade-off between convergence speed and tracking accuracy. The subsequent temperature study (25 - 70˚C) confirmed that this value remains sufficiently robust under thermal variations.

4) Compared to open-loop control with a fixed duty cycle (D = 0.50), the optimized P & O MPPT delivers a significant average power gain of +25.6%, reaching up to +39.3% at 25˚C.

5) The duty cycle adapts effectively from 0.375 at 25˚C to 0.49 at 70˚C, enabling robust retracking under temperature step changes.

These results confirm the critical importance of properly tuning the perturbation step in P & O algorithms when operating under thermal variations. However, the inherent limitations of the fixed-step P & O method, such as residual oscillations around the MPP and potential drift under rapid irradiance changes, highlight the need for further improvements.

Future work will focus on: (i) Experimental validation on a hardware prototype; (ii) Extension to partial shading conditions with global MPPT; (iii) Integration into a battery storage system; (iv) Implementation of an adaptive P & O algorithm based on the |ΔP/ΔV| gradient to simultaneously improve convergence speed and reduce steady-state oscillations; (v) Real-time experimental comparison between P & O, Incremental Conductance, and Fuzzy Logic controllers.

Author Contributions

Sada Traore conceived the study, developed the theoretical model, performed the numerical simulations, analyzed and interpreted the results, prepared the figures, and wrote the original manuscript. Moustapha Thiame contributed to the methodology, supervised the research, and critically revised the manuscript. Ansoumane Diedhiou contributed to the interpretation of the results and reviewed the manuscript. Modou Tine supervised the research, contributed to the scientific discussion, and critically revised the manuscript.

Conflicts of Interest

The authors declare no conflicts of interest regarding the publication of this paper.

References

[1] Ahmed, S., Ali, A., Ahmed Ansari, J., Abdul Qadir, S. and Kumar, L. (2025) A Comprehensive Review of Solar Photovoltaic Systems: Scope, Technologies, Applications, Progress, Challenges, and Recommendations. *IEEE Access*, **13**, 69723-69750. https://doi.org/10.1109/access.2025.3558539

[2] Rabaia, M.K.H., Abdelkareem, M.A., Sayed, E.T., Elsaid, K., Chae, K., Wilberforce, T., *et al.* (2021) Environmental Impacts of Solar Energy Systems: A Review. *Science of the Total Environment*, **754**, Article 141989. https://doi.org/10.1016/j.scitotenv.2020.141989

[3] Ali, M.H., Zakaria, M. and El-Tawab, S. (2025) A Comprehensive Study of Recent Maximum Power Point Tracking Techniques for Photovoltaic Systems. *Scientific Reports*, **15**, Article No. 14269. https://doi.org/10.1038/s41598-025-96247-5

[4] Ghribi, M.E.B., Garcia-Gutierrez, L., Ternifi, Z.E.T., Zheng, Z., Bachir, G. and Aillerie, M. (2024) Tracking the Maximum Power Point of Solar Panels through Direct Estimation of Optimum Voltage with Temperature. *Clean Energy*, **8**, 135-146. https://doi.org/10.1093/ce/zkae044

[5] Siddique, M.A.B., Zhao, D. and Rehman, A.U. (2025) Emerging Maximum Power Point Control Algorithms for PV System: Review, Challenges and Future Trends. *Electrical Engineering*, **107**, 9807-9839. https://doi.org/10.1007/s00202-025-03002-0

[6] Abdul Khani, N.A., Zakaria, M.I., Mat Yusoh, M.A.T., Kamarudin, M.N. and A.A Emhemed, A.R. (2024) Performance Evaluation of Solar Photovoltaic System Based on Perturb and Observe (P&O) Maximum Power Point Tracking (MPPT) Algorithm. *ESTEEM Academic Journal*, **20**, 135-146. https://doi.org/10.24191/esteem.v20iseptember.1593.g1826

[7] Jafar, M.I.A., Zakaria, M.I., Dahlan, N.Y., Kamarudin, M.N. and El Fezazi, N. (2024) Enhancing Photovoltaic System Maximum Power Point Tracking with Fuzzy Logic-Based Perturb and Observe Method. *International Journal of Electrical and Computer Engineering (IJECE)*, **14**, 2386-2399. https://doi.org/10.11591/ijece.v14i3.pp2386-2399

[8] Felita, A., Krisma, Y., Prabowo, P.S. and Harini, B.W. (2024) The Implementation of MPPT Perturb and Observe Method with Boost Converter on PV System. *AIP Conference Proceedings*, **3077**, Article ID: 050034. https://doi.org/10.1063/5.0201805

[9] Bahar, S.T. and Rashid, Y.G. (2024) A Study on an MPPT Control Approach Using Artificial Intelligence and the Perturb and Observe Method. *Diyala Journal of Engineering Sciences*, **17**, 131-143. https://doi.org/10.24237/djes.2024.17210

[10] Addawe, A., Mahmood, M.K., Karim, S.M. and Nezam, A.M. (2024) Analysis of Perturb and Observe MPPT under Varying PV Operating Climatic Conditions. 2024 21*st International Multi-Conference on Systems, Signals & Devices* (*SSD*), Erbil, 22-25 April 2024, 92-97. https://doi.org/10.1109/ssd61670.2024.10548879

[11] Nguyen-Duc, T., Nguyen-Duc, H., Le-Viet, T. and Takano, H. (2020) Single-Diode Models of PV Modules: A Comparison of Conventional Approaches and Proposal of a Novel Model. *Energies*, **13**, Article ID: 1296. https://doi.org/10.3390/en13061296

[12] Ukoima, K.N. (2025) A Comparative Analysis of the One, Two and Three-Diode Photovoltaic (PV) Models. *Solar Compass*, **16**, Article ID: 100144. https://doi.org/10.1016/j.solcom.2025.100144

[13] Pardhi, C., Khare, K. and Choubey, A. (2024) Impact of Irradiance and Temperature on Electrical Parameters of Polycrystalline Photovoltaic Module: A Five-Parameter Analysis. *International Journal of Recent Technology and Engineering*, **13**, 12-20. https://doi.org/10.35940/ijrte.B8085.13020724

[14] Chakiri, S. and Lamchich, M.T. (2021) Modelling Effect of Temperature and Irradiance Changes of Assa, Morocco on Photovoltaic Modules' Performance. *E3S Web of Conferences*, **240**, Article ID: 03005. https://doi.org/10.1051/e3sconf/202124003005

[15] Wester, G.W. and Middlebrook, R.D. (1973) Low-Frequency Characterization of Switched Dc-Dc Converters. *IEEE Transactions on Aerospace and Electronic Systems*, **9**, 376-385. https://doi.org/10.1109/taes.1973.309723

[16] Middlebrook, R.D. and Cuk, S. (1976) A General Unified Approach to Modelling Switching-Converter Power Stages. 1976 *IEEE Power Electronics Specialists Conference*, Cleveland, 8-10 June 1976, 18-34. https://doi.org/10.1109/pesc.1976.7072895

[17] Erickson, R.W. and Maksimovic, D. (2001) Fundamentals of Power Electronics. 2nd Edition, Kluwer Academic Publishers.

[18] Mohan, N., Undeland, T.M. and Robbins, W.P. (2003) Power Electronics: Converters, Applications, and Design. 3rd Edition, Wiley.

[19] Hohm, D.P. and Ropp, M.E. (2003) Comparative Study of Maximum Power Point Tracking Algorithms. *Progress in Photovoltaics: Research and Applications*, **11**, 47-62. https://doi.org/10.1002/pip.459

[20] Femia, N., Petrone, G., Spagnuolo, G. and Vitelli, M. (2005) Optimization of Perturb and Observe Maximum Power Point Tracking Method. *IEEE Transactions on Power Electronics*, **20**, 963-973. https://doi.org/10.1109/tpel.2005.850975

[21] Guerra, M.I.S., Ugulino de Araújo, F.M., Dhimish, M. and Vieira, R.G. (2021) Assessing Maximum Power Point Tracking Intelligent Techniques on a PV System with a Buck-Boost Converter. *Energies*, **14**, Article 7453. https://doi.org/10.3390/en14227453

[22] Endiz, M.S. (2023) Performance Analysis of P&O and PSO MPPT Algorithms for PV Systems under Partial Shading. *Konya Journal of Engineering Sciences*, **12**, 84-99. https://doi.org/10.36306/konjes.1359177

[23] Ahmad, M.E., Numan, A.H. and Mahmood, D.Y. (2022) A Comparative Study of Perturb and Observe (P&O) and Incremental Conductance (INC) PV MPPT Techniques at Different Radiation and Temperature Conditions. *Engineering and Technology Journal*, **40**, 376-385. https://doi.org/10.30684/etj.v40i2.2189

[24] Mahmod Mohammad, A.N., Mohd Radzi, M.A., Azis, N., Shafie, S. and Atiqi Mohd Zainuri, M.A. (2020) An Enhanced Adaptive Perturb and Observe Technique for Efficient Maximum Power Point Tracking under Partial Shading Conditions. *Applied Sciences*, **10**, Article 3912. https://doi.org/10.3390/app10113912

[25] Djilali, A.B., Bounadja, E., Yahdou, A., Benbouhenni, H., Elbarbary, Z.M.S., Colak, I., *et al.* (2025) Enhanced Variable Step Sizes Perturb and Observe MPPT Control to Reduce Energy Loss in Photovoltaic Systems. *Scientific Reports*, **15**, Article No. 11700. https://doi.org/10.1038/s41598-025-95309-y

[26] Ahmed, M., Abdelrahem, M., Harbi, I. and Kennel, R. (2020) An Adaptive Model-Based MPPT Technique with Drift-Avoidance for Grid-Connected PV Systems. *Energies*, **13**, Article 6656. https://doi.org/10.3390/en13246656

[27] Villegas-Mier, C.G., Rodriguez-Resendiz, J., Álvarez-Alvarado, J.M., Rodriguez-Resendiz, H., Herrera-Navarro, A.M. and Rodríguez-Abreo, O. (2021) Artificial Neural Networks in MPPT Algorithms for Optimization of Photovoltaic Power Systems: A Review. *Micromachines*, **12**, Article 1260. https://doi.org/10.3390/mi12101260

[28] Bresnav, K.V. and Singaravelu, S. (2026) Implementation and Dynamic Analysis (Variations in Irradiance) of MPPT Control Using Ann/Fuzzy Logic/P&O in a PV Power System for High Power Applications. *Discover Electronics*, **3**, Article No. 43. https://doi.org/10.1007/s44291-026-00169-z

[29] Boukenoui, R., Ghanes, M., Barbot, J.-P., Bradai, R., Mellit, A. and Salhi, H. (2017) Experimental Assessment of Maximum Power Point Tracking Methods for Photovoltaic Systems. *Energy*, **132**, 324-340. https://doi.org/10.1016/j.energy.2017.05.087

[30] Vidal-Martínez, R., García-Martínez, J.R., Rojas-Galván, R., Álvarez-Alvarado, J.M., Gozález-Lee, M. and Rodríguez-Reséndiz, J. (2025) A Review of Mamdani, Takagi-Sugeno, and Type-2 Fuzzy Controllers for MPPT and Power Management in Photovoltaic Systems. *Technologies*, **13**, Article 422. https://doi.org/10.3390/technologies13090422

[31] Almutairi, A., Abo-Khalil, A.G., Sayed, K. and Albagami, N. (2020) MPPT for a PV Grid-Connected System to Improve Efficiency under Partial Shading Conditions. *Sustainability*, **12**, Article 10310. https://doi.org/10.3390/su122410310

[32] Hussein, K.H., Muta, I., Hoshino, T. and Osakada, M. (1995) Maximum Photovoltaic Power Tracking: An Algorithm for Rapidly Changing Atmospheric Conditions. *IEE Proceedings-Generation, Transmission and Distribution*, **142**, 59-64. https://doi.org/10.1049/ip-gtd:19951577